Local Order of Amorphous Zeolite Precursors from $^{29}Si\{^1H\}$ CPMAS and ^{27}Al and ^{23}Na MQMAS NMR and Evidence for the Nature of Medium-Range Order from Neutron Diffraction

Huaixin Yang, Richard I. Walton,* Sasa Antonijevic, and Stephen Wimperis

Department of Chemistry, University of Exeter, Stocker Road, Exeter EX4 4QD, U.K.

Alex C. Hannon

ISIS Facility, Rutherford Appleton Laboratory, Chilton, Didcot, OX11 0QX, U.K.

Received: December 16, 2003; In Final Form: March 29, 2004

Amorphous aluminum silicates, isolated from hydrothermal reactions used to form crystalline zeolite A, have been studied using a number of techniques. NMR studies using $^{29}Si\{^1H\}$ cross-polarization (CP) MAS and ^{27}Al and ^{23}Na multiple-quantum (MQ) MAS methods provide information about the local atomic structure of the solids. Materials isolated at the early stages of reaction are silicon rich, and some of the aluminum is found in six-coordinate sites as in the amorphous alumina starting material. $^{29}Si\{^1H\}$ CPMAS NMR spectra show that a range of silicon environments are present in the amorphous solids. The line widths in the ^{27}Al MQMAS NMR spectra of the amorphous materials suggest that a range of Al−O distances and/or Si−O−Al angles is present, rather than the well-defined units present in zeolite A. Although the average ^{23}Na isotropic chemical shift suggests a coordination number of close to six for all sodium throughout the crystallization, the sodium in the amorphous precursor phase can be distinguished from that in the crystalline zeolite. The neutron diffraction study of the amorphous aluminosilicates reveals information about atomic order over longer length scales. The first sharp diffraction in the neutron diffraction data indicates, for the first time, that the medium-range order of the amorphous precursors changes prior to crystallization. The shift in the T−O peak (T is a tetrahedral atom: Si or Al) in the radial distribution function is consistent with the incorporation of aluminum into the silicate network at the early stages of reaction, and this is accompanied by the growth of an Na−O peak, as more charge-balancing cations are required. The broadness of the T--T nonbonded correlation for the amorphous solid, compared with that seen for crystalline zeolite A, indicates that there are no well-defined secondary building units present before the formation of zeolite crystals.

Introduction

The crystallization mechanism of microporous zeolites has attracted a great deal of attention for many years now, and has been widely reviewed; see, for example, refs 1−3. The diverse industrial uses of microporous solids in heterogeneous catalysis, ion exchange and gas separation give the materials huge commercial value and drive continued research into zeolite synthesis. More fundamental scientific interest in the materials also remains owing to the structural complexity of zeolites and the ability to include a huge variety of chemical elements in zeolitic frameworks to confer novel properties in the solid state.[4] Zeolite synthesis is often undertaken by a trial-and-error approach, involving variation of a large number of synthetic parameters until a new, crystalline material is produced in a pure state. This approach has been, and continues to be, highly productive, and it is believed that there remain many yet-undiscovered zeolite structures that will be synthesized in time.[5,6] Other research has addressed the question of zeolite crystallization mechanism with the hope of developing rational syntheses of new materials. A recent review by Cundy and Cox describes the development of the understanding of zeolite formation,[3] and it is apparent that since the 1960s a large body of literature has amassed that allows the steps in the formation of crystalline silicate zeolites to be described. There is still the need, however, to measure experimental data to verify the proposed pathways involved in the assembly of a zeolite structure; particularly data that concern the changes in atomic arrangement in the transformation of chemical reagents into a crystalline network structure.

Zeolites are most commonly synthesized using hydrothermal conditions, whereby chemical reagents, which might be solid or liquid, are heated in a sealed reaction container in an aqueous solution above 100 °C. For example, in the synthesis of an aluminum silicate zeolite, silica and alumina are mixed in the required ratio with a concentrated sodium hydroxide solution, and the mixture heated in a sealed reaction container for periods of hours to days. In recent years a number of elegant in situ X-ray and neutron scattering techniques have been developed that probe the changing long-range order of the solid state during hydrothermal zeolite crystallization under real reaction conditions,[7−10] and these have allowed new information concerning the transformation of starting materials into product to be obtained, such as accurate crystallization curves and the observation of crystalline intermediate phases. Wide-angle scattering techniques allow the development of long-range order to be determined by monitoring the appearance and growth of

* Corresponding author. E-mail: r.i.walton@exeter.ac.uk.

10.1021/jp037887g CCC: $27.50
Published on Web 05/21/2004

characteristic Bragg peaks (including those of any transient, crystalline phases[9]), whereas small-angle diffraction studies probe the growth (and decay) of small particles, prior to the appearance of crystallographic order.[11−13] The information lacking in these experiments is a probe of local, atomic structure during the transformation of starting materials to product. Although both solution and solid-state NMR experiments have been developed to study certain nuclei (such as ^{27}Al, ^{19}F, and ^{29}Si) under hydrothermal conditions,[14,15] the complexity of the experiment (requiring heated sample vessels under pressure) makes the method not generally applicable for in situ studies, in particular when the application of advanced, high-resolution NMR techniques would be desirable. To achieve some insight into this problem, we have studied the structures of disordered solids quenched from reacting mixtures of silica and alumina. We have studied the synthesis of zeolite A, because this is one of the most well-characterized zeolites and therefore represents a model system for investigation. After short reaction times it is well-documented that amorphous aluminosilicate phases are formed that on continued heating transform to the crystalline zeolite.[14,16−19] The local structure of these solids has been investigated previously using NMR spectroscopy,[16−18,20] but the development of new, high-resolution NMR methods for quadrupolar nuclei such as ^{23}Na and ^{27}Al has allowed us to study short-range atomic order in more detail than previously possible, and to examine for the first time the local environment of sodium using the ^{23}Na MQMAS NMR method. We have also undertaken what is to the best of our knowledge the first neutron diffraction study of the amorphous aluminosilicates: this allows us to determine the extent and the nature of medium-range order in the solids.

Experimental Section

Sample Preparation and Characterization. Zeolite A and its amorphous precursors were formed from a mixture of fumed silica (Sigma) and an amorphous aluminum oxide, prepared by thermal decomposition of aluminum nitrate hydrate (Aldrich) at 500 °C for 17 h. The solids were shaken together to achieve intimate mixing and stirred into a ∼1.95 M NaOH solution to produce a paste. Batches of the mixture, having final composition Al_2O_3:2 SiO_2:3.06 NaOH:128 H_2O, were placed in polypropylene bottles and heated at 100 °C for various periods of time (see below). Solids were recovered by suction filtration, washed with deionized water, and allowed to dry in air in a desiccator. Samples are labeled LTA$_n$, with n the reaction time (in hours) used to prepare the sample. For the neutron diffraction study, deuterated reagents were used: NaOD (Aldrich 40% in D_2O), D_2O (Fluorochem Ltd), and $Al_2O_3.nD_2O$ ($n \approx 0.5$) produced by standing freshly prepared amorphous Al_2O_3 in a D_2O atmosphere. The solids were analyzed using powder X-ray diffraction, recorded using a Bruker D8 diffractometer operating with Cu Kα radiation (average wavelength = 1.5418 Å). Powdered samples were pressed into aluminum sample holders and data collected in Bragg-Brentano geometry from 5 to 70° 2θ with a step-size of 0.02° 2θ and a counting time of 1 s per step. ICP analysis for aluminum and silicon was performed on selected samples by Medac Ltd, U.K.. The water content of the samples was determined using thermogravimetric analysis performed using a Stanton Redcroft TG750 thermal analyzer, with a ∼10 mg sample of each solid heated to 900 °C in air. The densities of all samples were measured using a Quantachrome Micropycnometer with helium as the working fluid. Energy-dispersive X-ray analysis (EDXA) was performed using scanning electron microscopy with an Electroscan 2020 environmental SEM; this was used to provide further elemental analysis by quantifying the relative intensities of characteristic emissions of Si, Al, and Na with crystalline zeolite A as a reference.

Solid-State NMR Studies. Spectra were recorded on a Bruker Avance 400 spectrometer equipped with a widebore 9.4 T magnet, operating at a Larmor frequency, ν_0, of 105.8 MHz for ^{23}Na ($I = 3/2$) and 104.3 MHz for ^{27}Al ($I = 5/2$), or on a Bruker Avance 200 spectrometer equipped with a widebore 4.7 T magnet, operating at $\nu_0 = 39.7$ MHz for ^{29}Si ($I = 1/2$). Samples were packed inside 4 mm (9.4 T) or 7 mm (4.7 T) rotors, and MAS rates were 10 and 5 kHz, respectively, were used. Cross-polarized (CP) ^{29}Si{^{1}H} MAS NMR spectra were recorded using a conventional cross-polarization sequence with ^{29}Si and ^{1}H radio frequency field strengths, $\nu_{1Si} = \nu_{1H}$, of ∼45 kHz and with a contact time of 3 ms. Chemical shifts are reported in ppm relative to an external standard of 0.15 M NaCl(aq) for ^{23}Na, 1.0 M $Al(NO_3)_3$(aq) for ^{27}Al, and TMS for ^{29}Si. Two-dimensional ^{23}Na and ^{27}Al triple-quantum MAS spectra were recorded using the z-filtered sequence of Amoureux et al.[21]

Solid-state NMR spectra of quadrupolar nuclei, i.e., those with spin quantum number $I > 1/2$, often have inherently low resolution owing to the presence of significant anisotropic quadrupolar broadening. This is a result of the interaction of the nuclear quadrupole moment (eQ) with the electric field gradient (eq). This quadrupolar coupling may be parametrized by its magnitude

$$C_Q = \frac{e^2qQ}{h} \tag{1}$$

and asymmetry, η, where $0 \le \eta \le 1$. In addition to the quadrupolar coupling, other mechanisms such as dipolar coupling or chemical shift anisotropy further increase the observed broadening, hindering the extraction of structural information. The use of magic angle spinning (MAS),[22] rotating the powdered sample about an axis inclined at 54.7° to the external magnetic field, removes the broadening to a first-order approximation, thereby significantly increasing the spectral resolution.

The quadrupolar interaction, however, may be very large (often of the order of megahertz), and in this case, its second-order effects result in anisotropic broadening that cannot be fully removed by MAS alone. The multiple-quantum MAS NMR technique (MQMAS),[23−25] offers a method for obtaining truly high-resolution spectra of half-integer spin ($I = 3/2$, $5/2$, etc.) quadrupolar nuclei through the removal of all anisotropic second-order quadrupolar broadening. The technique involves the two-dimensional correlation of multiple- and single-quantum coherences under MAS conditions. This results in a refocusing of the anisotropic quadrupolar broadening, whereas the isotropic chemical and quadrupolar shifts are retained. A two-dimensional Fourier transform yields a spectrum containing ridge line shapes that lie along a gradient equal to the MQMAS ratio, i.e., −7/9 for spin $I = 3/2$ and +19/12 for spin $I = 5/2$ for triple-quantum MAS.[23−25] A high-resolution spectrum may be obtained from a projection orthogonal to this axis. It is possible to obtain values of chemical shift and quadrupolar parameters from the two-dimensional spectra: the δ_1 and δ_2 positions of the center-of-gravity of a ridge line shape depend on both the isotropic chemical shift, δ_{iso}, and the isotropic quadrupolar shift, δ_Q. For spin $I = 3/2$ triple-quantum MAS spectra,[26]

$$\delta_1 = 3\delta_{iso} + (6/5)\delta_Q \tag{2}$$

$$\delta_2 = \delta_{iso} - (2/5)\delta_Q \tag{3}$$

and for spin $I = {}^5/_2$ triple-quantum MAS spectra,

$$\delta_1 = 3\delta_{iso} - (4/5)\delta_Q \quad (4)$$

$$\delta_2 = \delta_{iso} - (16/5)\delta_Q \quad (5)$$

Thus both δ_{iso} and δ_Q may be determined. The composite quadrupolar parameter,[27] $P_Q = C_Q(1 + \eta^2/3)^{1/2}$ may also be extracted from δ_Q:

$$P_Q = \frac{4I(2I-1)\nu_0\sqrt{\delta_Q}}{3000} \quad (6)$$

The quadrupolar parameters, C_Q and η, however, may not be obtained individually by this method.

For amorphous or disordered solids, MAS NMR is a valuable tool owing to its ability to probe local environment despite the lack of long-range order. The range of local environments encountered in such materials, however, leads to a distribution in the isotropic chemical shift and/or quadrupolar parameters of the nucleus studied.[28] This further broadens the spectrum and restricts the information available. The increased resolution offered by MQMAS makes it a useful technique for the study of amorphous and disordered materials and applications of ^{11}B ($I = {}^3/_2$), ^{17}O ($I = {}^5/_2$), ^{23}Na ($I = {}^3/_2$), and ^{27}Al ($I = {}^5/_2$) MQMAS to such systems may be found in the literature.[24,28−35] Ridge line shapes are rarely observed, owing to the distribution of shift parameters, but average values for δ_{iso} and P_Q can still be extracted by the center-of-gravity approach.

Neutron Diffraction Experiments. Neutron diffraction experiments were performed using the GEM diffractometer at ISIS, the UK spallation neutron source at the Rutherford Appleton Laboratory. GEM is a time-of-flight diffractometer that allows relatively rapid data collection owing to the large area of the detector banks (10 m^2, maximum azimuthal angle ~45°).[36] The time-of-flight method allows scattered neutrons to be measured to high values of momentum transfer, permitting high-resolution radial distribution functions to be obtained, which was considered important in the current work because we expected the materials to contain closely spaced atomic correlations. Powdered samples were loaded into 8 mm diameter vanadium cans and then dried gently in a vacuum oven at 70 °C to remove any residual protons due to surface water. The cans were then sealed before mounting in the diffractometer. The beam size was 40 × 15 mm, and data were collected from each sample for a period of ~5 h. A 6 mm vanadium rod was used to measure the incident energy spectrum, to normalize the time-of-flight data. The diffraction data were corrected using standard procedures for container and instrument scattering, attenuation, multiple scattering and inelasticity effects, using the ATLAS suite of programs.[37]

The quantity measured in the neutron diffraction experiment is the differential cross section:

$$\frac{d\sigma}{d\Omega} = I^S(Q) + i(Q) \quad (7)$$

where $I^S(Q)$ is the self-scattering, $i(Q)$ is the distinct scattering, and Q is the momentum transfer (the magnitude of the scattering vector). The first, which can be calculated with knowledge of the composition of the sample, is subtracted from the measured differential cross section to yield the distinct scattering. Fourier transformation then allows structural information to be obtained.

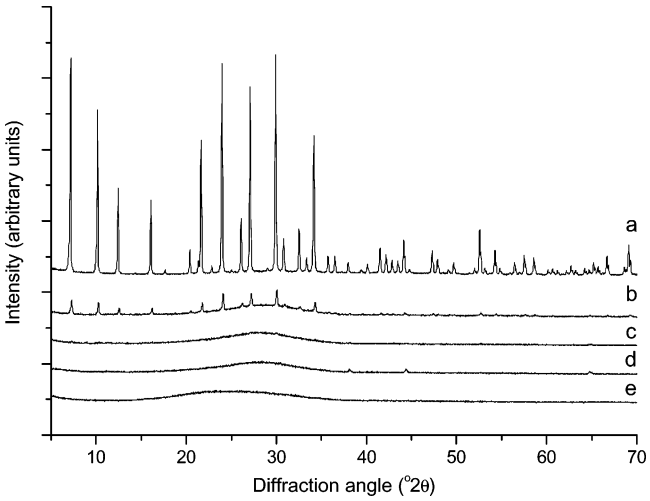

Figure 1. Laboratory powder X-ray diffraction patterns of aluminium silicates prepared after (a) 12, (b) 7, (c) 5, (d) 2, and (e) 0.5 h. Weak peaks at ~38, 44, and 65° 2θ in some of the patterns are due to the aluminium sample holder.

In this work we have reported the differential correlation function, $D(r)$:

$$D(r) = \frac{2}{\pi}\int_0^{Q_{max}} Q\, i(Q)\, M(Q) \sin(rQ)\, dQ \quad (8)$$

where r is the radial distance from an average origin atom. $M(Q)$ is a modification function, applied to reduce termination ripples caused by the finite extent of data used. In this work we have used the modification function due to Lorch:[38]

$$M(Q) = \frac{\sin(Q\Delta r)}{Q\Delta r} \quad \text{for } Q < Q_{max} \quad (9)$$

$$M(Q) = 0 \quad \text{for } Q > Q_{max} \quad (10)$$

where $\Delta r = \pi/Q_{max}$. Q_{max} is the maximum useful momentum transfer from the experimental data.

Results and Discussion

Laboratory Characterization and ^{29}Si{^{1}H} CPMAS NMR Spectra. Figure 1 shows powder X-ray diffraction data measured from the samples isolated after varying reaction times. The sole crystalline product after reaction times in excess of 12 h is zeolite A. All the peaks can be indexed with a refined cubic unit cell of $a = 24.544(8)$ Å (space group $Fm\bar{3}c$); this value agrees with previous structure determinations of the solid (it should be noted that unit cell volume of hydrated zeolite A is very similar to the dehydrated form).[39−42] If reaction times of shorter than 6 h are used, the solid isolated is amorphous. At slightly longer times the material contains crystalline zeolite A mixed with an amorphous phase. The Bragg peak widths due to zeolite A decrease slightly after their first appearance, suggesting that a period of crystal growth occurs at the crystallites first formed. These powder X-ray diffraction data are useful for determining, approximately at least, the extent of reaction with time but give no information about atomic arrangement in the solid state until the crystalline zeolite A appears. Table 1 contains the Si:Al ratios determined by ICP analysis for some of the samples, along with their water content determined by TGA, and their experimentally measured densities. As expected, zeolite A has a strict 1:1 Si:Al ratio, but it can be seen that at the early stages of reaction the amorphous

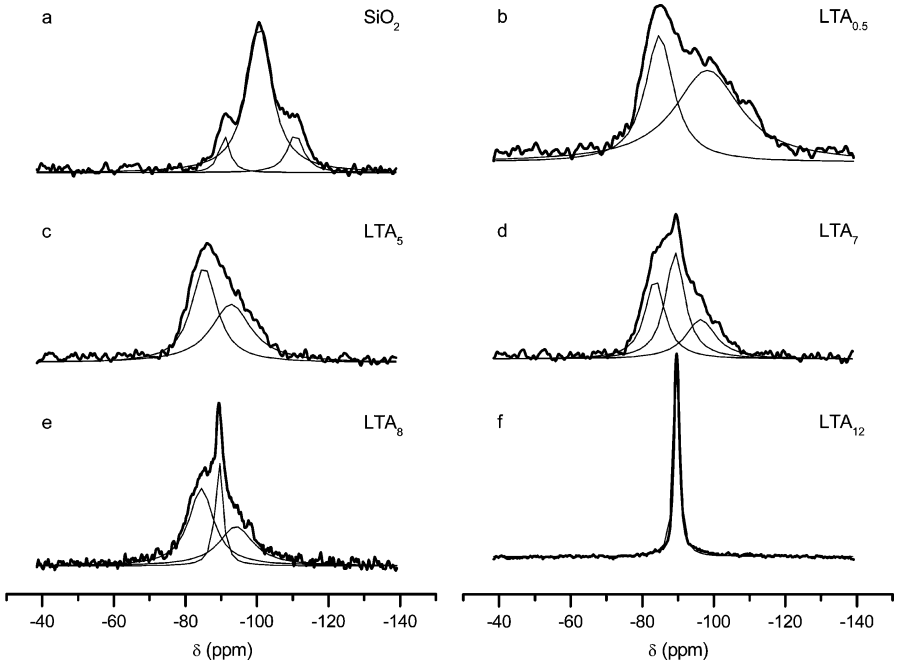

Figure 2. $^{29}Si\{^1H\}$ CPMAS NMR spectra of (a) fumed silica, (b) $LTA_{0.5}$, (c) LTA_5, (d) LTA_7, (e) LTA_8, and (f) LTA_{12}. The spectra are the result of averaging 2048 transients with a recycle interval of 5 s. The MAS rate was 5 kHz. The contact pulse duration was 3 ms.

TABLE 1: Reaction Times Used To Prepare Aluminum Silicates Studied and the Results of Analyses Performed[a]

sample	preparation time/h	Si/Al[b]	water content after air-drying (%)	density/ g cm^{-3}
$LTA_{0.5}$	0.5	2.7	15.5	1.56
LTA_2	2	1.8	17.4	2.11
LTA_5	5	1.6	17.8	2.11
LTA_7	7	1.4	17.3	1.99
LTA_{12}	12	1.0	22.3	2.01

[a] Time of reaction at 100 °C from an initial reaction mixture of composition Al_2O_3:2 SiO_2:3.06 NaOH:128 H_2O. Si/Al ratios are those determined by ICP analysis. [b] Estimated error on the Si:Al ratio is ±0.1, based on repeated analyses.

TABLE 2: Average Chemical Shift Values of Features Observed in the $^{29}Si\{^1H\}$ CPMAS NMR Spectra of the Materials Studied, Extracted by Fitting of Lorentzian Functions (See Figure 3)

sample	$\delta[^{29}Si]$ (ppm)
fumed silica	−110.7, −100.7, −91.0
LTA_0[a]	−109.1, −99.5, −88.9
$LTA_{0.5}$	−98.5, −85.0
LTA_2	−94.9, −85.5
LTA_5	−93.2, −85.3
LTA_7	−96.4, −89.2, −83.6
LTA_8[b]	−94.5, −89.4, −84.4
LTA_{12} (zeolite A)	−89.6

[a] Isolated after stirring the reagents at room temperature for 30 min. [b] Analysis results are similar to sample LTA_7.

solids formed are silicon rich. This is consistent with some previous studies of related materials; for example, Engelhardt et al. found that amorphous material with an Si:Al ratio of 2.4 formed at the early stages of the crystallization of zeolite A from sodium silicate and sodium aluminate solutions.[16,18] It should be noted that a direct comparison of the evolution of Si:Al ratio with reaction time between various previous studies is not valid, because the zeolite crystallization rate depends on many experimental factors, including temperature and specific choice of starting materials (including the particle size of solids used). We can make the general observation that at the early stages of reaction only a small amount of aluminum is incorporated into the silicate network with the remainder present as a soluble form. As the reaction proceeds, more aluminum is incorporated into the amorphous solid. The EDXA shows that the Al:Si ratio is similar in all particles analyzed in each sample, and also that the sodium content of the amorphous samples increases as more aluminum is incorporated: this is expected because the increasing negative charge of the aluminosilicate network must be balanced by more sodium cations.

Figure 2 shows $^{29}Si\{^1H\}$ CPMAS spectra measured from some of the amorphous materials, the fumed silica starting material and the crystalline zeolite A. The non-cross-polarized spectrum was also measured for sample LTA_8 to confirm the agreement in line shapes between the two methods. The CP method was then selected for its greater sensitivity. Table 2 contains the average chemical shift values of the main features observed in the $^{29}Si\{^1H\}$ CPMAS spectra for all of the materials studied. These were extracted by fitting with Lorentzian functions, as shown in Figure 2. The use of Gaussian functions would yield essentially identical results. ^{29}Si MAS NMR has been widely used to study zeolites and other aluminum silicates,[20,43] and the results of prior studies allow us to assign the observed features. For the crystalline zeolite A, a single resonance is observed, centered at $\delta = -89.6$ ppm, and this is typical of the material: for example, Engelhardt et al. report the resonance to be centered at $\delta = -89.4$ ppm[18] and Kulshreshtha et al. reported the same chemical shift value.[44] These values are typical of $Q^4(4Al)$ silicons.[43] The SiO_2 starting material contains three broad features centered at $\delta = -91.0$, -100.7, and -110.7 ppm. These spectral features are well-established for samples of fumed silica:[45,46] the last two features correspond to Q^3 and Q^4 silicon environments ($[Si-O]_3Si[OH]$ and $Si[O-Si]_4$) whereas the peak at -91 ppm is due to Q^2 silicons, i.e., those that have two surface hydroxyl groups attached ($[Si-O]_2Si[OH]_2$). For the amorphous material isolated at room temperature (after stirring the chemical reagents together for 30 min) the $Si\{^1H\}$ CPMAS spectra (not shown) show peaks centered at $\delta = -88.9$, -99.5, and -109.1 ppm, consistent with a network structure consisting largely of corner-shared silicate units with some surface silanol groups, similar to that seen in

the SiO_2 starting material. This indicates that only a trace of aluminum is incorporated into the solid after this short time and prior to heating the reagents.

After 0.5 h of reaction time there are at least two broad features: one at −98.5 ppm and the other centered at −85.0 ppm. The former is consistent with the presence of silicon-rich regions of sample, containing $Q^{2-4}(0Al)$ type silicons, as found in the starting material. The feature centered at −85 ppm may be assigned as arising from a broad range of $Q^n(mAl)$ silicons: the chemical shift range for $Q^2(mAl)$, $Q^3(mAl)$, and $Q^4(mAl)$ type silicons spans the range −75 to −100 ppm. Shi et al. studied a precursor to zeolite A and assigned peaks in the range −75 to −95 ppm to the same species,[14] Interestingly, Engelhardt et al. observed a single broad peak centered at −85.0 ppm for samples with an Si:Al ratio of 1:1, whereas for silicon-rich samples (Si:Al 2:1), the resonance is centered at −92.5 ppm.[16,18] Thus we propose that for our silicon-rich material prepared using the shortest of reaction times, a range of tetrahedral silicon sites are present: some as $Q^{2-4}(0Al)$ sites, where the network structure is siliceous, and some as $Q^{2-4}(mAl)$ where aluminum incorporation has taken place. The sample isolated after 5 h of reaction time is rather similar.

The samples isolated after 7 and 8 h of reaction time show the first sign of the sharp resonance at −89.6 ppm that is due to crystalline zeolite A [$Q^4(4Al)$], and weaker features at around −84 ppm and around −95 ppm still remain that are due to the amorphous component. This is complete agreement with the powder XRD data that show a mixture of zeolite A and amorphous material. Interestingly, the feature at close to −84 ppm, at higher ppm than the crystalline resonance, and which we attribute to $Q^3(3Al)$ type silicons, indicates that a significant number of Si−OH or Si−O^- moieties remain in the structure.

Although ^{29}Si MAS NMR has been widely applied to the study of zeolites and amorphous silicates, and our new ^{29}Si-{^{1}H} CPMAS data are similar to those previously reported for amorphous aluminosilicates, we can use the data to pinpoint changes in the local structure with increasing preparation time of the solids. In addition, our data are consistent with the observations from powder X-ray diffraction and provide a starting point for the interpretation of the remaining NMR data, and neutron diffraction data.

^{27}Al and ^{23}Na MQMAS NMR Spectra. Figures 3 and 4 show the ^{27}Al MAS and triple-quantum MAS NMR spectra recorded from the samples studied. The conventional MAS spectrum of the amorphous alumina starting material (not shown) indicates the presence of at least three distinct sites for aluminum; these have chemical shifts in the ranges expected for four-, five- and six-coordinated aluminum, which is consistent with the well-known observation that in samples of amorphous alumina a variety of coordination geometries are seen.[47] After the alumina and silica starting materials are stirred in sodium hydroxide solution at room temperature and the solid formed is recovered by filtration, the NMR data show evidence that much of the aluminum remains in octahedrally coordinated sites. The conventional MAS spectrum of this material indicates the presence of at least two distinct sites for aluminum in the solids, and the two-dimensional triple-quantum MAS NMR spectrum confirms the presence of two signals, albeit broadened as expected for an amorphous solid. One broad signal has an average isotropic chemical shift of 16.5 ppm, whereas the other is a complex signal made up of two components with average chemical shift values of 74.0 and 62.6 ppm. The first signal lies in the range expected for octahedrally coordinated aluminum, and the second, complex signal indicates tetrahedrally coordinated aluminum.[47]

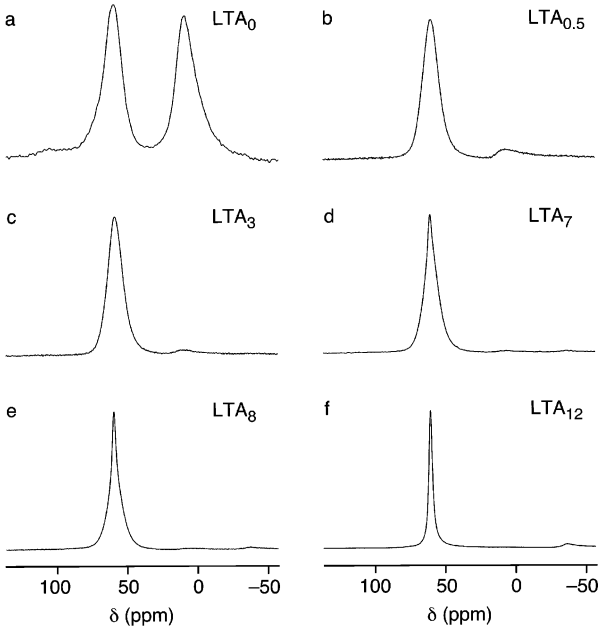

Figure 3. ^{27}Al MAS NMR spectra of (a) LTA_0, (b) $LTA_{0.5}$, (c) LTA_3, (d) LTA_7, (e) LTA_8, and LTA_{12}. The spectra are the result of averaging 320 transients with a recycle interval of 0.5 s. The MAS rate was 10 kHz.

The aluminum silicate sample isolated after 0.5 h of reaction time retains only a trace of octahedrally coordinated aluminum; one explanation for this is the presence of some unreacted amorphous alumina. The strongest signal, however, is that characteristic of tetrahedrally coordinated aluminum. All further samples contain solely tetrahedrally coordinated aluminum, but as progressively longer periods of heating are used, the signal becomes less broadened. For the sample isolated after 7 h of reaction time, the two-dimensional triple-quantum MAS NMR spectrum allows two distinct signals to be resolved: the conventional spectrum provides little evidence for the presence of these two signals, whereas in the two-dimensional spectrum a distinct "lobe" can be seen on the broad feature. One of these signals is broad and corresponds approximately to the signal of the amorphous material isolated at the beginning of the reaction, whereas the other is considerably sharper. Isotropic chemical shift values extracted from the two-dimensional spectra are given in Table 3. By examining the ^{27}Al triple-quantum MAS NMR spectrum of crystalline zeolite A and the P_Q values, we can see that the sharper signal in the sample isolated after 7 h of reaction time is due to the presence of the crystalline zeolite in the product mixture. The broadness of the signal of the amorphous materials indicates a range of Al−O bond distances or Al−O−Si angles are present, although the value of isotropic chemical shift is always in the region for tetrahedrally coordinated aluminum.

Figures 5 and 6 show the ^{23}Na MAS and triple-quantum MAS NMR spectra, respectively, of the amorphous materials. At a first glance the spectra show a single feature that is broadened to varying degrees, but a closer inspection reveals that the crystalline zeolite A exhibits a signal with an isotropic chemical shift value of 1.9 ppm, whereas for the first materials isolated, after stirring the reagents at room temperature, the signal is centered at 0.4 ppm. The fact that we only observe one resonance in the ^{23}Na NMR data, when there are three crystallographically unique sodium ions, is consistent with previous ^{23}Na studies of the zeolite: for example, Veeman and

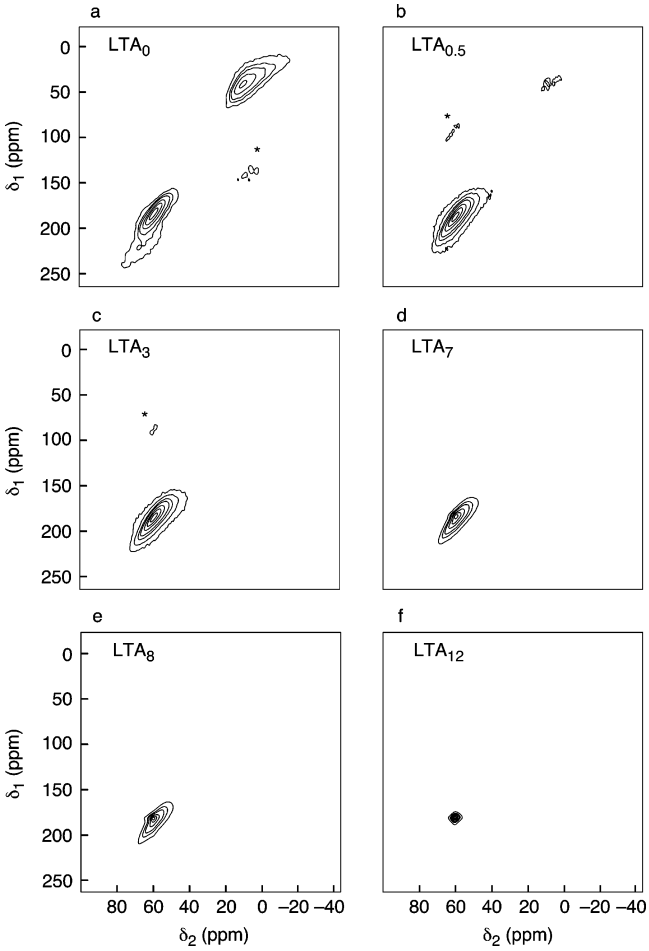

Figure 4. Two-dimensional ^{27}Al triple-quantum MAS NMR spectra of (a) LTA_0, (b) $LTA_{0.5}$, (c) LTA_3, (d) LTA_7, (e) LTA_8, and (f) LTA_{12}, recorded using a z-filtered pulse sequence. In (a) 576, (b)−(e) 144, and (f) 72 transients were acquired for each of (a)−(d) 128, (e) 256, and (f) 1024 t_1 increments of 8.33 μs. In each case, the recycle interval was 0.5 s and the MAS rate was 10 kHz. Contour levels are drawn at 4, 10, 20, 30, 50, 70, and 90% of the maximum value. Spinning sidebands are indicated by *.

TABLE 3: Average Isotropic Chemical Shifts (δ_{iso}) for ^{23}Na and ^{27}Al, Relative to 0.15 M NaCl(aq) and to 1.0 M $Al(NO_3)_3$(aq), Respectively, and Average Quadrupolar Products (P_Q) for Each Sample Studied, Extracted from Centers-of-Gravity of Two-Dimensional Triple-Quantum MAS NMR Line Shapes[a]

sample	δ_{iso}[^{27}Al] (ppm)	P_Q[^{27}Al] (MHz)	δ_{iso}[^{23}Na] (ppm)	P_Q[^{23}Na] (MHz)
LTA_0	74.0	4.4	0.4	1.6
	62.6	2.7		
	16.5	4.6		
$LTA_{0.5}$	64.3	3.0	−0.1	1.9
LTA_3	63.0	2.7	−0.7	2.0
LTA_7	63.0[b]	2.5[b]	2.0	1.3
			−0.2	2.0
LTA_8	63.0[b]	2.5[b]	1.5	1.3
			−0.6[b]	2.0
LTA_{12}	61.2	1.6	1.9	1.3

[a] Typical measurement errors in the values quoted are ±1.0 ppm (δ_{iso}) and ±0.3 MHz (P_Q). [b] Multiple sites were impossible to separate because of their close proximity (see Figure 4).

co-workers reported the same result in their ^{23}Na nutation NMR study of zeolite A hydration and suggested that the mobility of the sodium ions or water molecules, averages the three crystallographically unique sites.[48] For the materials isolated after

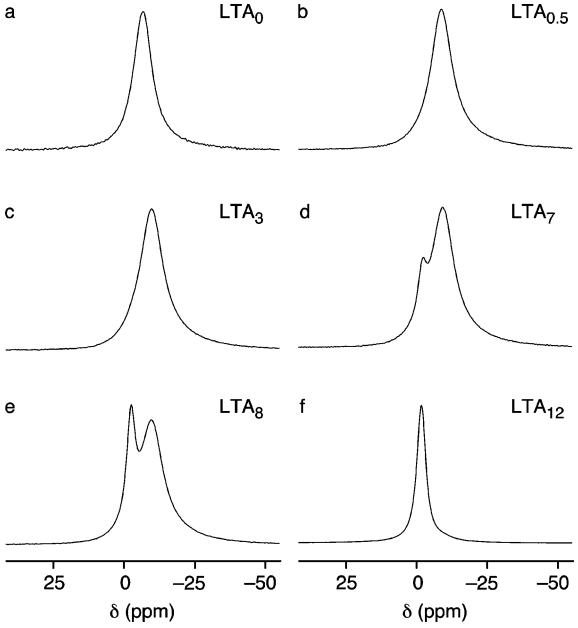

Figure 5. ^{23}Na MAS NMR spectra of (a) LTA_0, (b) $LTA_{0.5}$, (c) LTA_3, (d) LTA_7, (e) LTA_8, and (f) LTA_{12}. The spectra are the result of averaging 320 transients with a recycle interval of 0.5 s. The MAS rate was 10 kHz.

7 and 8 h of reaction time, the spectra contain signals characteristic of both the crystalline zeolite A and its amorphous precursor. To extract isotropic chemical shift values from spectra containing a complex signal made of more than one component, we simply estimated, by inspection, the position of each center-of-gravity; see Table 3. The validity of this approach was tested by extracting δ_{iso} and P_Q values from spectra that contained a single, symmetrical signal and comparing these with those extracted by a more rigorous approach based on numerical determination of the true center-of-gravity; excellent agreement was seen in these cases. The observation of two signals for samples LTA_7 and LTA_8 is consistent with the powder X-ray diffraction results, and the ^{27}Al triple-quantum MAS NMR spectra, but it is noteworthy that sodium in the crystalline and amorphous phases can be distinguished by NMR, even if the chemical environment of sodium in each phase is very similar. We have previously investigated whether any correlation exists between the ^{23}Na isotropic chemical shift and the local coordination environment of sodium in oxides by studying a range of solids that contain sodium in different environments.[35] We concluded that there is a general trend of increasing chemical shift with decreasing coordination number and average Na−O interatomic distance, which allows information about the coordination number and interatomic distance to be inferred, although the chemical shift is not an unambiguous parameter as it is for other nuclides, for example, ^{27}Al. The values of isotropic chemical shifts we see here for both the crystalline zeolite and its amorphous precursors are consistent with the presence of sodium bound to six oxygen atoms at 2.45−2.55 Å; sodium with fewer oxygen near-neighbors at shorter distances typically exhibits higher values of isotropic chemical shifts (up to 27 ppm).[35]

The local environment of sodium in dehydrated, crystalline zeolites is rather different than typically seen in many condensed solids, and often low coordination numbers and irregular geometries are found.[49] On hydration, however, the coordination number of sodium is increased by the presence of directly

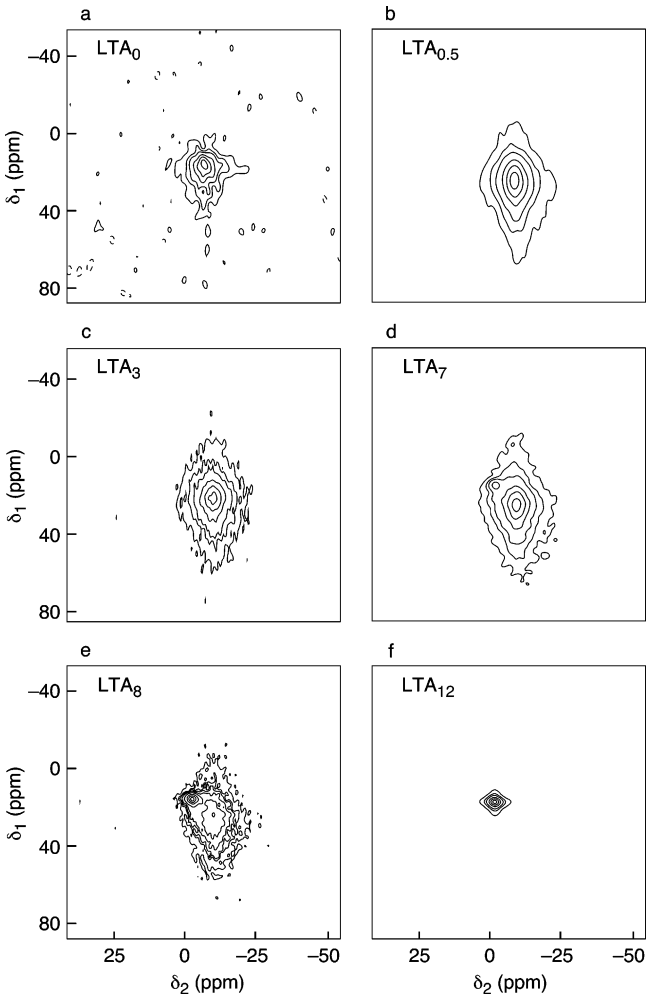

Figure 6. Two-dimensional ^{23}Na triple-quantum MAS NMR spectra of (a) LTA_0, (b) $LTA_{0.5}$, (c) LTA_3, (d) LTA_7, (e) LTA_8, and (f) LTA_{12}, recorded using a z-filtered pulse sequence. In (a)−(d), (f) 480 and (e) 384 transients were acquired for each of (a)−(d) 64 and (e), (f) 128 t_1 increments of 16.67 μs. In each case, the recycle interval was 0.5 s and the MAS rate was 10 kHz. Contour levels are drawn at 10, 20, 30, 50, 70, and 90% of the maximum value.

coordinating water molecules. Water in zeolite cages is often disordered, and the electron density due to its presence is usually modeled as a number of sites having fractional occupancy; this makes the identification of the precise local environment of sodium ions difficult. A number of structure determinations of zeolite A have been undertaken over the years,[39−41,49] but the most useful for us to consider are those by Ikeda et al. who studied both dehydrated and hydrated zeolite A using a combination of powder diffraction and maximum-entropy methods.[42] For dehydrated zeolite A, three crystallographically unique sodium ions are coordinated to either three or four framework oxygen atoms (at distances between 1.9 and 2.9 Å) and reside in positions close to the center of the four-, six-, and eight-membered rings. On hydration, the sodium ions migrate closer to the center of the α and β cages, i.e., away from the windows, and water molecules lie very close to the cations.[42] The coordination of each of the sodium ions then increases to, on average, between 5 and 6 (this includes both framework oxygens and water molecules), and these oxygen atoms lie at distances between 1.9 and 2.9 Å. The upper value is perhaps too large to be considered a chemical bond, but these oxygens are nevertheless rather close to the sodium ions and must be considered as part of the chemical environment of the ions. Interestingly, Pluth and Smith suggested that the long Na−O distances in hydrated zeolite A observed by X-ray diffraction are a consequence of framework vibration, and the "real" Na−O distances are lower than the values taken between centroids of electron density.[49]

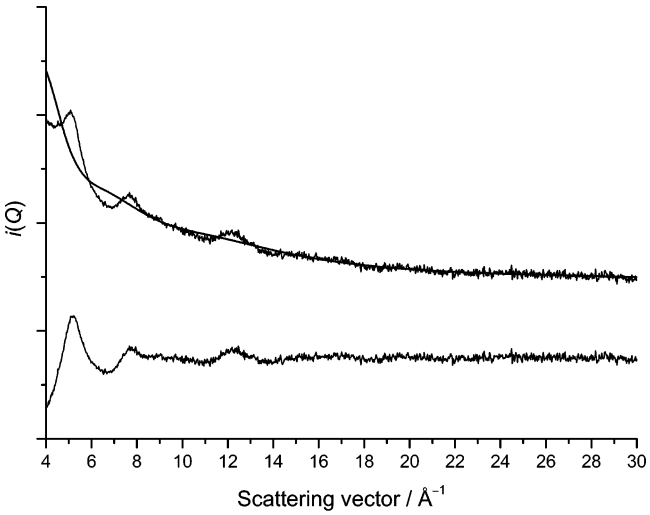

Figure 7. Correction of the raw neutron scattering data (GEM 90° detector bank) from sample LTA_5 for the incoherent scattering of residual protons for data from one GEM bank. Note that for this detector bank, data in the range 8−30 Å^{-1} were used to produce the complete $i(Q)$.

Our new ^{23}Na NMR data are thus consistent with the presence of 5- or 6-coordinate sodium ions in the hydrated, crystalline zeolite A, and also in the amorphous aluminum silicates, because the value of δ_{iso} is always between +2.1 and −1.6 ppm. Our results are in agreement with the widely accepted crystallization model for the formation of many zeolites, in which hydrated sodium ions, $Na(H_2O)_n^+$ ($n \approx 6$ for the first coordination shell) act as templates for the building up of the aluminosilicate network.[3] Sodium remains coordinated to around 6 oxygen atoms throughout the crystallization process.

Neutron Diffraction Data. The samples for the neutron diffraction experiment were prepared using deuterated reagents to avoid the large incoherent scattering background due to the presence of protons. Although our samples were dried carefully, they apparently exchange water with the atmosphere readily because all samples exhibit the characteristic sloping background of the incoherent scattering due to the presence of some protons. For most materials it is possible to perform a successful calculation of the Q-dependence of the self-scattering, $I^s(Q)$, by use of a Placzek correction[50] that takes into account the effects of inelasticity within an approximation.[51,52] However, for samples that contain very light nuclei, especially hydrogen and deuterium, the effects of inelasticity are too severe and the approximation breaks down. Instead, the self-scattering can be subtracted from the differential cross section by an empirical approach whereby a smooth, nonoscillatory function is fitted to the data.[53,54] In this work we have used a cubic spline with a variable knot spacing to perform this correction. Figure 7 shows such a correction for the data from one of the detector banks on GEM (note that each detector bank does not measure the full extent of scattering data, and overlapping regions of data from each bank are used, so that a nonoscillatory background is always fitted).

Figure 8 shows the distinct scattering, $i(Q)$, for each of the amorphous samples studied, along with that of crystalline zeolite A, plotted to 20 Å^{-1} to allow comparison. The most striking feature of the functions is their overall similarity (ignoring the sharp Bragg peaks of zeolite A), suggesting that the network

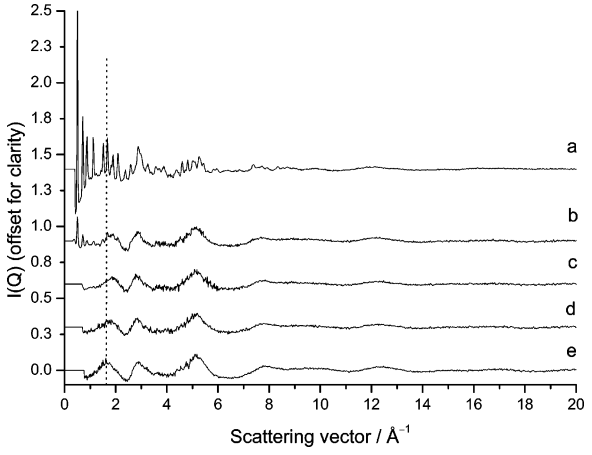

Figure 8. Distinct scattering, $i(Q)$, for samples (a) LTA_{12}, (b) LTA_7, (c) LTA_5, (d) LTA_2, and (e) $LTA_{0.5}$. The dotted line indicates the variation of the position of the first sharp diffraction peak between samples.

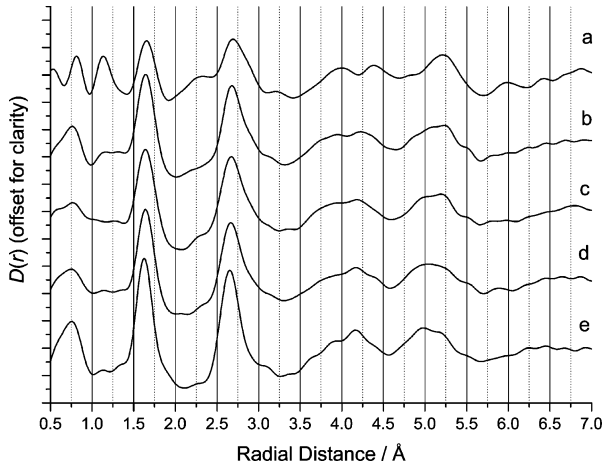

Figure 9. The differential correlation function, $D(r)$, for samples (a) LTA_{12}, (b) LTA_7, (c) LTA_5, (d) LTA_2, and (e) $LTA_{0.5}$.

structure of the amorphous materials resembles to some extent that of the final crystalline product. A closer inspection of the data, however, does reveal some subtle differences, even between the amorphous samples prepared using the shortest reaction times. The "first sharp diffraction peak", indicated in Figure 8, is observed to shift depending on the preparation time of the samples, and this is particularly noticeable between the amorphous materials LTA_2 and LTA_5. This diffraction feature is widely supposed to arise from the presence of medium-range order (i.e., beyond the first few coordination shells of each atom, extending between 5 and 20 Å), although it is extremely difficult to extract quantitative information regarding order over such length scales.[55,56] Our data thus provide the first indication that although the local atomic structure probed by NMR is rather similar for the amorphous zeolite precursors, particularly in terms of coordination number, their structure does change prior to zeolite crystallization.

To extract quantitative information from the neutron diffraction regarding the atomic arrangement in the amorphous materials, radial distribution functions were produced by Fourier transformation of the interference function according to eq 8 and using $Q_{max} = 30$ Å^{-1}. Figure 9 shows the differential correlation function, $D(r)$, for each of the materials studied. Note that any peaks below 1 Å are not physically meaningful and are probably due to some residual background that has not been corrected fully. Once again, an initial comparison indicates that

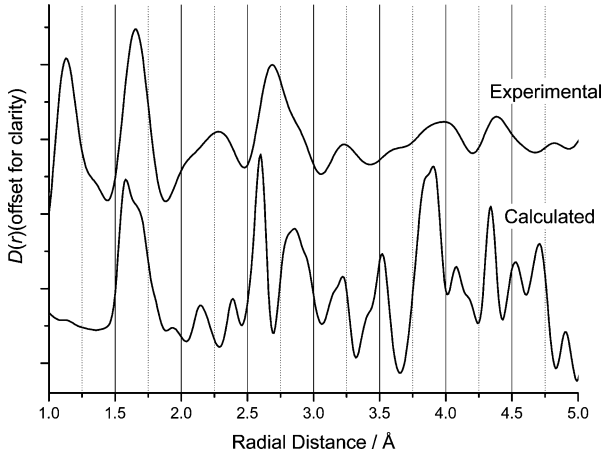

Figure 10. Calculated $D(r)$ for crystalline, hydrated zeolite A using the structural model of Ikeda et al. and comparison with the experimental function (see Table 4 for assignment of peaks).

each of the solids has a similar atomic arrangement, because peaks in the radial distribution occur at similar positions and have similar relative intensities for each material. A detailed examination of the data, however, reveals significant changes taking place with increasing sample preparation time: for example, it can be seen that the first peak in $D(r)$ (at around 1.6 Å) shifts with increasing sample preparation time, the relative intensity of a peak at ~3.2 Å changes with time, and in the region 3.5−5 Å significant changes are observed. To assign these peaks to specific atomic pairs and understand their variation from sample to sample, we consider previous crystal structures of zeolites and relate this to our experimental correlation function for the crystalline material.

The shortest interatomic separation expected in zeolite A will be that of the O−H pair at ~1 Å due to the presence of occluded water molecules. It should be noted that the relative height of the O−H/D peak in the $D(r)$ function will be affected severely by the relative amount of protons and deuterons in the sample: because H and D neutron scattering lengths have opposite signs, −3.74 and +6.67 fm, respectively,[57] the O−D and O−H contributions will tend to cancel each other. (Note that all isotopes of the other elements in the samples have positive scattering lengths.) Despite the many structural investigations of zeolite A, there is no full description of its structure that includes all proton positions for the fully hydrated material, but we can examine the crystal structures of other hydrated zeolites to provide reference distances for O−H/D bonds. The peak we see in $D(r)$ of zeolite A lies at 1.14 Å, and this compares well with O−D distances determined by neutron diffraction in the zeolites sodalite[58] (1.06 Å), hydroxosodalite[59] (0.90−1.15 Å), zeolite Y[60] (0.98 and 1.14 Å), and laumonite[61] (0.95−1.21 Å). It should be noted that the first three zeolites here are sodium aluminum silicates whose structure is made up from the same sodalite cage that is seen in zeolite A, so these provide very good systems for direct comparison with zeolite A.

Figure 10 shows the calculated $D(r)$ from the crystal structure of hydrated zeolite A determined by Ikeda et al. from powder X-ray diffraction data.[42] The $D(r)$ calculation was performed using the program XTAL[62] using a constant peak broadening of 0.04 Å. The structure solution of Ikeda et al. for $Na_{95}Si_{97}Al_{95}O_{384}(H_2O)_{248}$ is the most complete available for any hydrated sample of zeolite A, although their structural model does not include any proton positions and only the positions of oxygen atoms of water molecules (as well as sodium cations and framework atoms). Our material has a similar composition: between $Na_{97}Si_{97}Al_{97}O_{384}(H_2O)_{221}$ and $Na_{97}Si_{97}Al_{97}O_{384}(D_2O)_{199}$,

TABLE 4: Selected Radial Distances in Hydrated Zeolite A (from the Crystal Structure Determination of Ikeda et al.)[42] That Have Been Used To Interpret the Correlation Functions of the Amorphous Solids[a]

radial distance (Å)	atomic correlation
1.59	Si−O
1.73	Al−O
2.10−2.90	Na−O
2.20−2.90	O--O (hydrogen-bonded water molecules)
2.60−2.75	O--O (within tetrahedral units)
2.80−3.00	O--O (water-framework atoms)
3.20−3.25	T--T
3.20−3.80	Na--T

[a] T represents a tetrahedral center (aluminum or silicon). A nonbonded atomic correlation is indicated by --.

based on all chemical analysis results. The agreement between the experimental $D(r)$ for our sample of zeolite and the calculated curve is most informative. It must be noted that the relative intensities of peaks in the measured $D(r)$ is affected by the finite Q range of the data,[62] but the positions of major peaks show agreement. The O−D/H peak at 1.14 Å that we observe experimentally is clearly not predicted by the model of Ikeda et al. (which contains no H/D positions), but all other significant peaks in the experimental D(r) are accounted for by this model. The contribution of atomic correlations that include H/D must be responsible to some extent for discrepancies between the model, where they are not included, and the measured data (particularly given the large amount of H_2O/D_2O in the samples) and it is also likely that there is a large degree of disorder for the proton positions in the samples. Nevertheless, the comparison of the functions for crystalline zeolite A is valuable because it allows us to assign the peaks seen in $D(r)$ plots, and then to infer information about order in the amorphous solids. Table 4 lists the peak assignments made by direct comparison of the calculated and experimental functions.

The second distinct peak in the $D(r)$ functions can be assigned to Si−O and Al−O pairs (T−O, in general): these are expected to occur at 1.59 and 1.73 Å, respectively, in hydrated zeolite A.[42] The position of this first peak in $D(r)$ shifts as increasing reaction time is used to prepare the samples: from 1.63 Å for $LTA_{0.5}$ to 1.65 Å for LTA_{12}. This is entirely consistent with the elemental analysis showing the materials prepared after the shortest period of time to be silicon rich; thus the average T−O distance is initially somewhat shorter. For a material with an Si:Al ratio of 3:1 (close to that of the amorphous sample prepared using the shortest reaction time) the average T−O distance is expected to be 1.625 Å, and for a material with a Si:Al ratio of 1:1, 1.66 Å. The next sharp peak in the $D(r)$ functions lies at ∼2.4 Å and by using the above NMR results and the zeolite A crystal structure, this can be assigned as arising from the closest Na−O contacts. This peak becomes more intense (relative to the T−O peak) as increasing reaction time is used, which is entirely consistent with the fact that as more aluminum is incorporated into the solid, more sodium must be present to balance the net negative charge of the network. This result indicates that the amorphous network is made up of $\{AlO_4\}$ and $\{SiO_4\}$ units. It should also be noted that intermolecular O--O distances between hydrogen-bonded water molecules are expected to occur at 2.4 Å in zeolite A[42] and so must also contribute toward the intensity of this peak.

The complex, intense peak in $D(r)$ at ∼2.75 Å contains a large component due to O--O pairs within $\{TO_4\}$ tetrahedral units (T = Al or Si), expected at 2.6 Å; and this is well-known for materials constructed from tetrahedral primary building units.[55] This peak overlaps with peaks due to O--O pairs between water molecules and framework oxygens (∼2.8−3.0 Å). The similar positions of these peaks in all samples shows the similarity of the short-range order in all samples, but it should be noted that this peak broadens to the higher radial distance side as crystallization proceeds. This can be simply interpreted as arising from a greater amount of $Na(H_2O)_6^+$ within the solid, consistent with the decreasing Si:Al ratio, and the water analysis results (see Table 1); thus a larger number of O--O pairs between water and framework oxygens are present.

A very important atomic correlation to consider is that due to neighboring tetrahedral centers (Si--Al in a 1:1 aluminum silicate), because this gives information about the average T−O−T angle, and thus the presence of different secondary building units. In zeolite A, which is constructed solely of four- and six-membered rings, the shortest T--T distances are found at ∼3.2 Å, and this peak is indeed observed in the radial distribution function. (It should be noted that Na--T distances are seen at similar distances in zeolite A, so these will also contribute to the radial distribution in this region.) It is noteworthy that for the amorphous materials the T--T peak at ∼3.2 Å is of much lower intensity than the O--O peak at 2.75 Å in $D(r)$. This suggests that the amorphous material is made of a variety of structural units; rings of a variety of sizes, and perhaps aluminosilicate chains, which possess a variety of T−O-T angles and hence T--T distances. This is not true for all zeolite crystallizations: for example, Twu et al. in their vibrational spectroscopy study of the formation of mordenite observed four- and five-membered rings in the amorphous precursor gel.[63] For zeolite A, there is no evidence for a preponderance of units with specific T--T correlations until the long-range order, characteristic of the zeolite, is present.

As we examine the $D(r)$ to higher radial distance, interpretation becomes more difficult, because peaks become increasingly overlapped with their neighbors. It is important to note, however, that the region 3−5 Å in $D(r)$ begins to resemble that of the crystalline zeolite for the amorphous materials prepared with the longer reaction times (LTA_5, for example), whereas for the silicon-rich solids isolated at the early stages of reaction, the medium-range order is rather different. This appears to show that considerable structural rearrangement of the amorphous phase takes place even prior to the formation of zeolite crystals.

Conclusions

The amorphous materials isolated from reactions used to prepare zeolite A have local atomic order that resembles that of the crystalline zeolite. The use of sensitive solid-state NMR methods has provided new information about the solids. For example, by studying the ^{23}Na MQMAS spectra, we can ascertain that hydrated sodium ions are present at all stages of crystallization, and that despite having a similar chemical shift throughout the crystallization process, sodium in crystalline and amorphous phases can be distinguished in mixtures of the two. To the best of our knowledge our neutron diffraction data are the first measured from amorphous zeolite precursors. Despite the complexity of the system (five chemical elements and ready exchange with atmospheric water), we are able to detect the presence of medium-range order in the amorphous materials and relate this to the structure of the crystalline zeolite finally produced. Our work has highlighted the absence of complete structural models for hydrated zeolites, and this must be the subject of future work: it is possible that total diffraction measurements might have a role to play in solving this problem. At the present time, even without knowledge of H/D positions,

we can obtain information about the structure of the amorphous aluminosilicate network and its interaction with the charge-balancing hydrated sodium cations.

We have studied solid phases isolated from zeolite crystallizations, but it is also important to bear in mind the role of the solution in crystallization. It has been established that zeolite crystallization may occur via homogeneous routes (for example, from clear solutions by dissolution of starting materials and/or intermediate phases) or by heterogeneous processes (directly from the amorphous precursor gel by interaction with the solution). Thus methods that probe the structure of the solution will always be important in providing complementary information about zeolite crystallization.[19,64] In situ scattering studies of the heterogeneous mixtures present during crystallization would obviously be extremely desirable, but the data from a mixture of solution and solid, both of changing composition, would be extremely difficult to interpret

Further interpretation of the neutron scattering data is extremely complex, and even for binary systems, such as SiO_2, only with advanced computer modeling methods and models containing hundreds of atoms can the subtle features in the radial distribution functions be accounted for. Nevertheless, for our system (which contains five chemical elements) the assignment of peaks by direct comparison with an appropriate crystalline material allows us to interpret the data from the amorphous solids, providing valuable, new information about the presence and nature of medium-range order in these materials. A noteworthy result is that there is no evidence for the presence of distinct secondary building units in the amorphous materials prior to the formation of the zeolite. This result is consistent with some previous solution NMR studies of aluminosilicate solutions taken from zeolite crystallization that show the presence of simple monomeric or dimeric units rather than the building units found in the crystalline solid.[65,66] The amorphous solids we have studied may be thought of as reservoirs for the reactive solution species that allow zeolite crystal growth but are not actually built up of only the secondary building units found in the zeolite itself.

Acknowledgment. We thank the Royal Society for the award of a K. C. Wong Fellowship to H.X.Y., the EPSRC for funding (GR/N07622), and the CCLRC for provision of beamtime at ISIS. We are grateful to Dr. S. E. Ashbrook of the Department of Earth Sciences, University of Cambridge, for advice on the interpretation of the ^{29}Si NMR data and to Mr. J. Hawkins of the Interface Analysis Centre, University of Bristol, for the EDXA.

References and Notes

(1) Barrer, R. M. *Hydrothermal Chemistry of Zeolites*; Academic Press: London, 1982.
(2) Francis, R. J.; O'Hare, D. *J. Chem. Soc., Dalton Trans* **1998**, 3133.
(3) Cundy, C. S.; Cox, P. A. *Chem. Soc. Rev.* **2003**, *103*, 663.
(4) Cheetham, A. K.; Ferey, G.; Loiseau, T. *Angew. Chem., Int. Ed. Engl.* **1999**, *38*, 3268.
(5) Klinowski, J. *Curr. Opin. Solid State Mater. Sci.* **1998**, *3*, 79.
(6) Newsam, J. M.; Bein, T.; Klein, J.; Maier, W. F.; W, W. S. *Microporous Mesoporous Mater.* **2001**, *48*, 355.
(7) Norby, P. *J. Am. Chem. Soc.* **1997**, *119*, 5215.
(8) Cheetham, A. K.; Mellot, C. F. *Chem. Mater.* **1997**, *9*, 2269.
(9) Walton, R. I.; O'Hare, D. *Chem. Commun.* **2000**, 2283.
(10) Walton, R. I.; Smith, R. I.; O'Hare, D. *Microporous Mesporous Mater.* **2001**, *48*, 79.
(11) Dougherty, J.; Iton, L. E.; White, J. W. *Zeolites* **1995**, *15*, 640.
(12) Kirschhock, C. E. A.; Ravishankar, R.; Jacobs, P. A.; Martens, J. A. *J. Phys. Chem. B* **1996**, *103*, 11021.
(13) Moor, P. P. E. A. d.; Beelen, T. P. M.; Santen, R. A. v.; Beck, L. W.; Davis, M. E. *J. Phys. Chem. B* **2000**, *104*, 7600.
(14) Shi, J. M.; Anderson, M. W.; Carr, S. W. *Chem. Mater.* **1996**, *8*, 369.
(15) Gerardin, C.; Haouas, M.; Lorentz, F.; Taulelle, F. *Magn. Reson. Chem.* **2000**, *38*, 429.
(16) Engelhardt, G.; Fahlke, B.; Magi, M.; Lippmaa, E. *Zeolites* **1983**, *3*, 292.
(17) Müller, D.; Starke, P.; Jank, M.; Wendlandt, K.-P.; Bremer, H.; Scheler, G. *Z. Anorg. Allg. Chem.* **1984**, *517*, 167.
(18) Engelhardt, G.; Fahlke, B.; Mägi, M.; Lippmaa, E. *Zeolites* **1985**, *5*, 49.
(19) Serrano, D. P.; Grieken, R. V. *J. Mater. Chem.* **2001**, *11*, 2391.
(20) Bell, A. T. *Colloids Surf. A: Phys. Eng. Asp.* **1999**, *158*, 221.
(21) Amoureux, J. P.; Fernandez, C.; Steuernagel, S. *J. Magn. Reson. A* **1996**, *123*, 116.
(22) Andrew, E. R.; Bradbury, A.; Eades, R. G. *Nature* **1958**, *182*, 1659.
(23) Frydman, L.; Harwood, J. S. *J. Am. Chem. Soc.* **1995**, *117*, 5367.
(24) Fernandez, C.; Amoureux, J. P. *Solid State Nucl. Magn. Reson.* **1996**, *5*, 315.
(25) Brown, S. P.; Wimperis, S. *J. Magn. Reson.* **1997**, *128*, 42.
(26) Bodart, P. R. *J. Magn. Reson.* **1998**, *133*, 207.
(27) Mueller, K. T.; Baltisberger, J. H.; Wooten, E. W.; Pines, A. *J. Phys. Chem.* **1992**, *96*, 7001.
(28) Kentgens, A. P. M. *Geoderma* **1997**, *80*, 271.
(29) Hunger, M.; Sarv, P.; Samoson, A. *Solid State Nucl. Magn. Reson.* **1997**, *9*, 115.
(30) Stebbins, J. F.; Oglesby, J. V.; Xu, Z. *Am. Mineral.* **1997**, *82*, 1116.
(31) Hwang, S. J.; Fernandez, C.; Amoureux, J. P.; Han, J. W.; Cho, J.; Martin, S. W.; Pruski, M. *J. Am. Chem. Soc.* **1998**, *120*, 7337.
(32) Angeli, F.; Charpentier, T.; Faucon, P.; Petit, J. C. *J. Phys. Chem. B* **1999**, *103*, 10356.
(33) McManus, J.; Ashbrook, S. E.; MacKenzie, K. J. D.; Wimperis, S. *J. Non-Cryst. Solids* **2001**, *282*, 278.
(34) Ashbrook, S. E.; McManus, J.; MacKenzie, K. J. D.; Wimperis, S. *J. Phys. Chem. B* **2000**, *104*, 6408.
(35) Antonijevic, S.; Ashbrook, S. E.; Walton, R. I.; Wimperis, S. *J. Mater. Chem.* **2002**, *12*, 1469.
(36) Hannon, A. C. In *Encyclopedia of Spectrsocopy and Spectrometry*; Lindon, J., Tranter, G., Holmes, J., Eds.; Academic Press: London, 2000; Vol. 2, p 1479.
(37) Hannon, A. C.; Howells, W. S.; Soper, A. K. *IOP Conf. Ser.* **1990**, *107*, 193.
(38) Lorch, E. *J. Phys. C* **1969**, *2*, 229.
(39) Gramlich, V.; Meier, W. M. *Z. Kristallogr.* **1971**, *133*, 134.
(40) Cheetham, A. K.; Eddy, M. M.; Jefferson, D. A.; Thomas, J. M. *Nature* **1982**, *299*, 24.
(41) Adams, J. M.; Haselden, D. A.; Hewit, A. W. *J. Solid State Chem.* **1982**, *44*, 245.
(42) Ikeda, T.; Izumi, F.; Kodairi, T.; Kamiyama, T. *Chem. Mater.* **1998**, *10*, 3996.
(43) *Handbook of Porous Solids*; Schüth, F., Sing, K. S. W., Weitkamp, J., Eds.; Viley-VCH: Weinheim, 2002; Vol. 1, p 478.
(44) Kulshreshtha, S. K.; Vijayalakshami, R.; Sudarsan, V. *Stud. Surf. Sci. Catal.* **1998**, *113*, 699.
(45) Liu, C. C.; Maciel, G. E. *J. Am. Chem. Soc.* **1996**, *118*, 5103.
(46) Maciel, G. E.; Sindorf, D. W. *J. Am. Chem. Soc.* **1980**, *102*, 7606.
(47) Kunath-Fandrei, G.; Bastow, T. J.; Hall, J. S.; Jäger, C.; Smith, M. E. *J. Phys. Chem.* **1995**, *99*, 15138.
(48) Tijink, G. A. H.; Janssen, R.; Veeman, W. S. *J. Am. Chem. Soc.* **1987**, *109*, 7301.
(49) Pluth, J. J.; Smith, J. V. *J. Am. Chem. Soc.* **1980**, *102*, 4704.
(50) Placzek, G. *Phys. Rev.* **1985**, *86*, 377.
(51) Howe, M. A.; McGreevy, R. L.; Howells, W. S. *J. Phys. Condens. Matter.* **1989**, *1*, 3433.
(52) Wright, A. C. *J. Non-Cryst. Solids* **1985**, *76*, 187.
(53) Farman, H.; Blakey, D.; Dore, J. C.; Bellissent-Funel, M.-C.; Elliott, S. R. *Phys. Scripta* **1994**, *49*, 634.
(54) Yanwei, Z.; Fagherazzi, G.; Polizzi, S. *J. Mater. Sci.* **1995**, *30*, 2153.
(55) Elliott, S. R.; Rao, C. N. R.; Thomas, J. M. *Angew. Chem., Int. Ed. Engl.* **1986**, *25*, 31.
(56) Elliott, S. R. *Nature* **1991**, *354*, 445.
(57) *International Tables for Crystallography*; Kluwer Academic Publishers: Dordrecht, 1995; Volume C.
(58) Felsche, J.; Luger, S.; Fischer, P. *Acta Crystallogr. C* **1987**, *43*, 809.
(59) Wiebcke, M.; Engelhardt, G.; Felsche, J.; Kempa, P. B.; Sieger, P.; Schefer, J.; Fischer, P. *J. Phys. Chem.* **1992**, *96*, 392.
(60) Czjek, M.; Jobic, H.; Fitch, A. N.; Vogt, T. *J. Phys. Chem.* **1992**, *96*, 1535.
(61) Stahl, K.; Artioli, G. *Eur. J. Mineral.* **1993**, *5*, 851.
(62) Hannon, A. C. Rutherford Appleton Laboratory Report RAL-93-063, 1993.
(63) Twu, J.; Dutta, P. K.; Kesge, C. T. *J. Phys. Chem.* **1991**, *95*, 7.
(64) Davies, M. E.; Lobo, R. F. *Chem. Mater.* **1992**, *4*, 756.
(65) Knight, C. T. G. *Zeolites* **1990**, *10*, 140.
(66) Swaddle, T. W. *Coord. Chem. Rev.* **2001**, *219*−*221*, 665.